Low-frequency Sound Propagation Modeling Over a Locally-reacting Boundary Using the Parabolic Approximation

by

J.S. Robertson, W.L. Siegmann

and M.J. Jacobson

NAG-1-929

Department of Mathematical Sciences

Rensselaer Polytechnic Institute

Troy, New York 12180-3590

RPI Math. Rep. No. 175

August 31, 1989

This work is sponsored by

National Aeronautics and Space Administration

Langley Research Center

Research Grant No. NAG-1-929

ABSTRACT

There is substantial interest in the analytical and numerical modeling of low-frequency, long-range atmospheric acoustic propagation. Ray-based models, because of frequency limitations, do not always give an adequate prediction of quantities such as sound pressure or intensity levels. However, the parabolic approximation method, widely used in ocean acoustics, and often more accurate than ray models for lower frequencies of interest, can be applied to acoustic propagation in the atmosphere. Modifications of an existing implicit finite-difference implementation for computing solutions to the parabolic approximation are discussed. A locally-reacting boundary is used together with a one-parameter impedance model. Intensity calculations are performed for a number of flow resistivity values in both quiescent and windy atmospheres. Variations in the value of this parameter are shown to have substantial effects on the spatial variation of the acoustic signal.

INTRODUCTION

The propagation of low-frequency sound through the earth's atmosphere over long distances near the ground surface is a problem with numerous applications. For example, the propagation through winds of a low-frequency noise field generated by large wind turbines has been extensively studied both theoretically and experimentally.[1] In addition, low-frequency sound can be used to detect, locate and track aircraft or vehicles with passive acoustic sensors.[2,3]

In many instances, acoustic propagation occurs in environments which may be characterized by winds, atmospheric turbulence, extremes of weather, and other natural and man-made atmospheric variations, as well as irregular topography and terrain structure. These environmental variations are typically range- as well as height-dependent, and can profoundly affect the behavior of sound waves. Geometrical acoustics, or classical ray theory, is one approach that has been applied widely to the study of atmospheric acoustics. Unfortunately, the approximations under which the ray equations hold are valid only for sufficiently high source frequencies. At lower frequencies where diffraction effects are especially important, the use of other mathematical models can provide more accurate and useful results. Models, such as parabolic approximations[4] and the fast-field program[5] are more appropriate for use at frequencies where diffractive effects are non-negligible. Of these two approaches, the method of parabolic approximation is well-suited for handling range-dependent environments and has been applied to examine atmospheric propagation in a number of studies.[6-10] Originally formulated to examine tropospheric radio wave propagation, and successfully applied to a broad variety of problems in ocean acoustics, parabolic approximations exploit characteristic features of the propagation medium associated with the formation of a waveguide. Atmospheric acoustic waveguides can be created by certain meteorological conditions either with or without boundary interaction. Within such a waveguide, sound waves may propagate to relatively large distances with significant amplitudes.

While many studies have focussed attention on calculating the sound field propagation

over an impedance boundary, (e.g. see Refs. 11 and 12 and the references contained therein), relatively few have been concerned with low-frequency (10 to 100 Hz), long distance (5 or more km) propagation along the ground surface.[13-15] Reference 13 examined the sensitivity of attenuation variations to changes in both the atmospheric boundary layer and ground surface composition while phase effects were considered in Ref.14. An exact analytical model using normal modes was obtained in Ref. 15. For two examples of the extensive literature treating long-range propagation of infrasound away from the ground, see Refs. 16 and 17. References 18 and 19 examined high-frequency sound fields through a wind over an impedance plane, while Ref. 20 formulated an analytical solution to long-distance, low-frequency propagation, but over a perfectly reflecting ground. In Ref. 7, an asymptotic solution to the parabolic approximation is developed and analyzed along an impedance boundary, but no numerical implementation was discussed. On the other hand, Ref. 9 included refraction from both temperature and wind effects, and developed a finite element PE implementation, but the emphasis in that study was on relatively high frequencies and moderate ranges.

In this paper, we are concerned principally with developing a numerical model which can be used to conduct parametric studies of low-frequency cw propagation over an impedance boundary in a windy atmosphere over substantially long ranges. As noted above, relatively little computational work has addressed this problem. In Sec. I we briefly review the development of the parabolic approximation in a moving atmosphere, and then we discuss implementation details of the boundary conditions and other technical issues. Numerical simulations for propagation in quiescent and windy atmospheres are discussed in Sec. II, and the results of the paper are summarized in the last section.

I. MODEL FORMULATION

Let $p(r, z)$ be the acoustic pressure caused by the presence of a point source in a stratified, moving atmosphere, where r and z denote the range and height in cylindrical coordinates. We will confine our attention to a vertical plane containing the source, and parallel to the

wind motion. In addition, we assume that the sound speed is independent of azimuth, so that we deal only with two-dimensional sound propagation. The time-independent wave field, denoted as $A(r,z)$, is obtained by assuming that the source is harmonic with frequency f, so that $p = A\exp(2\pi i f t)$, where t is time. In the source receiver plane, it can be shown[21] that A satisfies the reduced wave equation

$$\nabla^2 A + k_0^2 n^2 A + 2ik_0^2 n^2 \frac{v}{c_0} A_r - 2i\frac{k_0}{c_0}\frac{dv}{dz} A_{zr} = 0, \tag{1}$$

where c_0 is a reference sound speed, $k_0 = 2\pi f/c_0$ is a reference wave number, $c(r,z)$ is the sound speed, $n(r,z) = c_0/c(r,z)$ is the index of refraction, and $v(z)$ is the wind speed. Furthermore, it can be shown that away from the source, the quantity A takes on the asymptotic form

$$A = \psi \frac{e^{ik_0 r}}{\sqrt{k_0 r}}. \tag{2}$$

Equation (2) is an essential feature of the parabolic approximation, where the quantity ψ is related to the slow-scale (i.e. many-wavelength) variation in the acoustic pressure. In addition, through careful scaling and asymptotic arguments, it can also be shown that ψ satisfies one of a family of parabolic equations (PEs). Details of the derivation of this family of PEs in an inhomogeneous moving medium can be found in Refs. 21 and 22. For the numerical examples considered in the next section, the appropriate member of this family is given by

$$2ik_0\psi_r + \psi_{zz} + k_0^2(\tilde{n}^2 - 1)\psi = 0, \tag{3}$$

where

$$\tilde{n} = c_0/\tilde{c}, \tag{4}$$

with

$$\tilde{c} = c + v. \tag{5}$$

The quantity $\tilde{c}$ is called the *effective sound speed profile* (ESSP).[21]

We assume that the ground surface is a locally reacting boundary. Although not strictly true in many cases, nevertheless this assumption has been shown repeatedly to be reasonably

accurate.[23] Such a boundary, when horizontal, is modeled by the following equation:

$$\psi_z|_{z=0} + ik_0\beta\psi|_{z=0} = 0, \tag{6}$$

where β is the normalized surface admittance (reciprocal of impedance). For the remainder of this paper, we will use the Delaney-Bazley-Chessell (DBC) impedance model:[23]

$$\beta^{-1} = 1 + 9.08(f/\sigma)^{-0.75} - i11.9(f/\sigma)^{-0.73}, \tag{7}$$

where σ is the flow resistivity in cgs units (g cm^{-3} s^{-1}). We emphasize that *any* alternative single or multi-parameter impedance model could be used as well.[27] The DBC model has the advantage of being simple to implement and widely used.

The usual PE starting field requires some modification. In contrast to the method used in Ref. 9, we insert an image source beneath the locally-reacting ground surface and require that the sum of the image field and source field satisfy the boundary condition given by Eq. (6). The point source and its image in the plane are modeled here by the function $G(z, z_s)$ where

$$G(z, z_s) = \sqrt{\frac{k_0}{2}} \exp\{-[k_0(z - z_s)/2]^2\}, \tag{8}$$

where z_s is the height above the bottom boundary. Let $g(z) = \psi(0, z) = G(z, z_s) + \gamma G(z, -z_s)$. Substituting this into Eq. (6) yields

$$\gamma = \frac{k_0 z_s - i\beta}{k_0 z_s + i\beta}. \tag{9}$$

As $\beta \to 0$, $\gamma \to 1$, which yields an image source with the expected amplitude over a perfectly-reflecting boundary. As $\beta \to \infty$, $\gamma \to -1$, and this produces the correct behavior of the image source across a pressure-release boundary. [In fact, this special case of the boundary condition has been previously implemented for ocean applications in which the source was close to the sea surface.[24]]

II. SIMULATION RESULTS

Our implementation of Eqs. (3) and (6) is based upon IFD, the implicit finite difference model described in Ref. 24. That model, together with the numerous modifications and

enhancements described by us here and elsewhere,[25,26] shall be referred to as the NASA Implicit Finite Difference (NIFD) model. The Crank-Nicholson scheme used to march the solution forward in range is well-suited for many propagation situations, for example, those involving locally reacting surfaces or irregularly-shaped boundaries. From this algorithm, we determine ψ, then A from Eq. (2) is the complex-valued pressure field, and finally relative intensity $I(r,z)$, defined as

$$I = 20 \log_{10} \left| \frac{A(r,z)}{A_{\text{ref}}} \right|, \tag{10}$$

where p_{ref} is the pressure at 1 m from the source. Figure 1 depicts an idealized atmospheric acoustic waveguide. We note here that this waveguide is similar to one used as a model in Ref. 1, a study of the downwind propagation of low frequency noise from a wind turbine located at a test site in Wyoming. A cw sound source is located $h_S = 40$ m above a horizontal, locally-reacting ground surface. The receiver will be located on the ground surface for all examples. The air is assumed to be isospeed with $c_0 = 330$ m s^{-1}. The atmosphere will be taken in Subsection B to move within the indicated plane with a logarithmic velocity profile, a modeling assumption often used for the vertical structure of winds:

$$v = 0.4 v_f \log_{10} \left(1 + \frac{z}{z_0} \right), \tag{11}$$

where $v_f = 14$ m s^{-1} is a strong but reasonable value for the free-stream wind speed, and $z_0 = 0.1$ m is characteristic thickness of the boundary layer (a similar profile was used in Refs. 1 and 9). Once the free stream velocity is achieved, the wind speed is held fixed for further increases in height z. As shown, the channel is bounded above by a horizontal, artificial, pressure-release surface of height h, beneath which is an artificial absorbing layer of thickness 500 m. This absorbing layer is designed to eliminate reflections that would otherwise occur from the pressure-release surface at the top of the waveguide. This technique is used to simulate bottom boundary conditions in ocean acoustics,[24] and, modified by us as described here, is a feature of NIFD, the numerical implementation which we use for our calculations.

A. No Wind

An exact solution to the sound field of a point source over an impedance plane in a quiescent, isothermal ($c_0 = 330$ m s^{-1}) atmosphere[12] can be used to check the accuracy of our implementation. Figure 2 depicts the exact solution calculated with flow resistivity $\sigma = 1000$ (an acoustically hard surface) compared against our PE solution in two ways. The solid curve represents the solution when the artificial boundary is at a height of 1000 m above the ground, while the dashed curve is computed when it is 2000 m above the ground. The dotted curve is the exact solution. Note that near the ground, which is that part of the atmosphere with which we are concerned here, all three calculations are in very close agreement. For the solid curve, the absorbing layer begins at height 500 m, and the effect of this layer is seen at this height. The higher artificial surface, whose absorbing layer begins at height 1500 m, extends the accuracy even higher as seen in the dashed curve. For very low values of flow resistivity, the PE is still accurate as seen in Fig. 3. In this example, $\sigma = 10$ (an acoustically soft surface). For several hundred meters above the ground, the three solutions are in very close agreement, which is where we require the accuracy. Figures 2 and 3 illustrate the accuracy of our locally-reacting boundary implementation as well as the effectiveness of the upper boundary condition.

A detailed picture of the sound field from a source with frequency 10 Hz when no wind is present can be seen in Fig. 4. In this and all remaining examples, $c_0 = 330$ m s^{-1}. Relative intensity as a function of range r is shown for four values of the flow resistivity σ. Values of σ shown have been measured by researchers in the field.[28,29] Roughly, $\sigma = 1000$ corresponds to very hard-packed earth, while a flow resistivity of 250 might be encountered over a soil consisting of sandy loam. A value of $\sigma = 50$ might be found on ground surfaces under cultivation, while a new-fallen snow cover could yield values of σ near 10. Our choices of flow resistivity values attempt to capture a variety of ground surfaces. In the figure, note that intensity decreases as σ decreases. Equivalently, a cw signal experiences additional attenuation as the surface impedance (admittance) decreases (increases). At longer ranges, even a 10 Hz signal can encounter substantial additional attenuation over very soft ground surfaces. As seen in Fig. 5, the effect of ground impedance obtained from the DBC model

is stronger for a signal one octave up, at $f = 20$ Hz. For a very hard surface, the change in intensity is small, but as σ decreases, the intensity decrease for the 20 Hz signal can be much stronger than for the 10 Hz one. For example, with $\sigma = 250$, the intensity decreases 3 dB with a doubling of frequency. When $\sigma = 10$, the 20 Hz signal is nearly 10 dB lower. We note here that this general trend continues as frequency increases.

B. Downwind

For the remaining examples, the receiver is located downwind from the source using the wind profile in Eq. (11) with parameters discussed previously. With this geometry, the effective sound-speed increases with height, so that sound waves tend to be refracted towards the ground surface. As a consequence, a waveguide is formed at the ground surface, and intensity levels can be enhanced significantly. In Fig. 6, we see a 10 Hz signal propagating over four different impedance boundaries in the wind profile. For large values of flow resistivity, there is very little structure present in the intensity curve. However, as σ decreases, an interference pattern begins to emerge, and it most pronounced when $\sigma = 10$.

Impedance effects on the interference structure are even more pronounced in the next illustration in Fig. 7. For $f = 20$ Hz, we begin to see substantial multipath effects occur even over very hard ground surfaces as depicted in Fig. 7. As the flow resistivity decreases, there is not only a decrease in overall intensity level (as was seen in Fig. 5), but the interference structure shifts markedly. In fact, if the interference pattern is though of as beating modes, it is evident from Fig. 7 that the higher-order mode is being attenuated at a faster rate for smaller values of the flow resistivity. In fact for $\sigma = 10$ multipath effects seem to be very weak. These kinds of shifts can have interesting practical consequences. For example, acoustic systems designed to detect and track low-flying aircraft could find their performance affected as the system is moved from place to place. Even systems deployed at a fixed installation could encounter a substantial degradation in effectiveness after a heavy snowfall. In applications for which source-receiver ranges are fixed, such as the design of noise control barriers, the acoustic propagation pattern could be "tuned" in some sense, by altering the

ground surface through cultivation or planting. In any case, it is apparent that winds (or other focusing phenomena) can influence sound interaction with locally-reacting ground surfaces in interesting ways.

As the source frequency increases, more complex dependence of the received field on impedance emerges. As displayed in Fig. 8, when $f = 40$ Hz an additional propagation mode is clearly seen to emerge for $\sigma = 1000$. As the flow resistivity decreases, the intensity curves not only experience a decrease in level, but a noticeable smoothing also occurs. This stripping of the highest-order mode(s) appears to be strongest within the transition from $\sigma = 1000$ to $\sigma = 250$. Also, note that the intensity peaks and nulls appear to be less sharply pronounced at 40 Hz than at 20 Hz.

At $f = 80$ Hz the tendency to strip modes seems to be lessened as flow resistivity decreases. In Fig. 9 there is a very strong interference pattern present over the acoustically-hardest ground surface. Peaks and nulls are very well-defined, and bear similarities more with Fig. 7 than with Fig. 8. As σ decreases to 250 there is a drop in the intensity level but the interference structure seems to remarkably well-preserved At $\sigma = 50$ there is a noticeable change in pattern, while for the softest ground surface, there appears to be a noticeable change in the interference pattern, and some obvious mode stripping has occurred.

SUMMARY

We have described an implementation of an implicit finite-difference method for solving the parabolic approximation in the atmosphere over a locally-reacting boundary. This model handles upper the radiation condition, and utilizes the Delaney-Bazley-Chessell impedance model. We present calculations in both quiescent and windy atmospheres. Solutions obtained from our implementation are shown to agree well with exact solutions for the sound field over an impedance plane in an isospeed, quiescent atmosphere. As the source frequency increases in octaves from 10 Hz to 80 Hz, variations in the flow resistivity can produce marked changes in the multipath interference structure of the downwind sound field. In general, lower resistivities (higher ground admittances) tend to strip off higher-order modes, which can

cause substantial changes in both the location and magnitude of intensity peaks and nulls. We emphasize that this numerical implementation has the potential to handle significantly more complicated environments, which might include irregular ground topography and range-dependent sound speed conditions in the medium.

[1] J.A. Hawkins, "Application of ray theory to propagation of low frequency noise from wind turbines," NASA Langley Res. Center, Hampton, VA (1987), CR-178367.

[2] F. Dommermuth and J. Schiller, "Estimating the trajectory of an accelerationless aircraft by means of a stationary acoustic sensor," J. Acoust. Soc. Am. **76**, 1114–1122 (1984).

[3] F. Dommermuth, "The estimation of target motion parameters from cpa time measurements in a field of acoustic sensors," J. Acoust. Soc. Am. **83**, 1476–1480 (1988).

[4] S.M. Candel, "Sound source radiation in two-dimensional shear flow," AIAA J. **21**, 221–227 (1983).

[5] R. Raspet, S.W. Lee, E. Kuester, D.C. Chang, W.F. Richards, R. Gilbert, and N. Bong, "A fast-field program for sound propagation in a layered atmosphere above an impedance ground," J. Acoust. Soc. Am. **77**, 345–353 (1985).

[6] M.K. Myers and G.L. McAninch, "Parabolic approximation for sound propagation in the atmosphere," AIAA J. **16**, 836–842 (1978).

[7] G.L. McAninch and G.K. Myers, "Propagation of quasiplane waves along an impedance boundary," in *Proceedings, AIAA 26th Aerospace Sciences Meeting* (AIAA, Washington, 1988).

[8] J.S. Robertson, M.J. Jacobson, and W.L. Siegmann, "Mathematical modeling of sound propagation in the atmosphere using the parabolic approximation," Transactions of the Sixth Army Conference on Applied Mathematics and Computing (1989)

[9] K. Gilbert and M. White, "Application of the parabolic equation to sound propagation in a refracting atmosphere," J. Acoust. Soc. Am. **85**, 630–637 (1989).

[10] P. Malbéqui and F. Jouaillec, "Acoustic propagation over the ground using the parabolic approximation," to appear in *Proceedings, INTERNOISE 88.*

[11] C.F. Chien and W.W. Soroka, "Sound propagation along an impedance plane," J. Sound Vib. **43**, 9–20 (1975).

[12] M.A. Nobile and S.I. Hayek, "Acoustic propagation over an impedance plane," J. Acoust. Soc. Am. **78**, 1325–1336 (1985).

[13] A.I. Otrezov and I.P. Chunchuzov, "The amplitude distribution of a low-frequency sound field near the surface of the earth," Izv. Atmos. Ocean. Phys. **23**, 76–78 (1987).

[14] T.N. Nesterova, A.I. Otrezov, A.S. Smirnov, and I.P. Chunchuzov, "Effect of temperature and wind stratification in the bottom layer of the atmosphere on the phase of low-frequency sound waves," Izv. Atmos. Ocean. Phys. **23**, 157–158 (1987).

[15] W.E. Zorumski and W.L. Willshire, "The acoustic field of a point source in a uniform boundary layer over an impedance plane," in *Proceedings, AIAA 26th Aerospace Sciences Meeting* (AIAA, Washington, 1988).

[16] L. Liszka, "Long-distance propagation of infrasound from artificial sources," J. Acoust. Soc. Am. **56**, 1383–1388 (1974).

[17] L. Liszka, "Temporal variations of long distance propagation of infrasound," J. Low Freq. Noise Vib. **7**, 1–6 (1988).

[18] D.C. Pridmore-Brown, "Sound propagation in a temperature- and wind-stratified medium," J. Acoust. Soc. Am. **34**, 438–443 (1962).

[19] V. Ye. Ostashev, "High-frequency acoustic field of a point source lying above an impedance surface in a stratified moving medium," Izv. Atmos. Ocean. Phys. **23**, 370–377 (1987).

[20] I.P. Chunchuzov, "Field of a low-frequency point source of sound in an atmosphere with a non-uniform wind-height distribution," Sov. Phys. Acoust. **30**, 323–327 (1984).

[21] J.S. Robertson, W.L. Siegmann, and M.J. Jacobson, "Current and current shear effects in the parabolic approximation for underwater sound channels," J. Acoust. Soc. Am. **77**, 1768–1780 (1985).

[22] J.S. Robertson, W.L. Siegmann, and M.J. Jacobson, "Acoustical effects of ocean current shear structures in the parabolic approximation," J. Acoust. Soc. Am. **82**, 559–573 (1987).

[23] C.I. Chessell, "Propagation of noise along a finite impedance boundary," J. Acoust. Soc. Am. **62**, 825–834 (1977).

[24] D. Lee and S.T. McDaniel, "Ocean acoustic propagation by finite difference methods," Comp. & Maths. with Appls. **14**, 305–423 (1987).

[25] J.S. Robertson, D.C. Arney, W.L. Siegmann, and M.J. Jacobson, "An efficient enhancement of finite-difference implementations for solving parabolic equations," J. Acoust. Soc. Am. **86**, 252–260 (1989).

[26] J.S. Robertson, D.C. Arney, W.L. Siegmann, and M.J. Jacobson, "Adaptive numerical enhancements to finite-difference algorithms for parabolic approximations," to appear in *Proceedings, Second IMACS Symposium on Computational Acoustics.*

[27] K. Attenborough, "Acoustical impedance models for outdoor ground surfaces," J. Sound Vib. **99**, 521–544 (1985).

[28] R. Raspet, H.E. Bass, and J. Ezell, "Effect of finite ground impedance on the propagation of acoustic pulses," J. Acoust. Soc. Am. **74**, 267–274 (1983).

[29] K. Attenborough, "Review of ground effects on outdoor sound propagation from continuous broadband sources," Appl. Acoust. **24**, 289–319 (1988).

FIGURE LEGENDS

FIG. 1. Atmospheric sound channel.

FIG. 2. Height z vs. relative intensity I for exact solution and two NIFD computations; no wind is present; $f = 10$ Hz, $\sigma = 1000$.

FIG. 3. Height z vs. relative intensity I; Same as Fig. 2 except $\sigma = 10$.

FIG. 4. Relative intensity I vs. range r for different values of flow resistivity σ; no wind present; $f = 10$ Hz.

FIG. 5. Relative intensity I vs. range r; same as Fig. 4 except $f = 20$ Hz.

FIG. 6. Relative intensity I vs. range r; 14 m s^{-1} wind present, receiver is downwind; otherwise same as in Fig. 4.

FIG. 7. Relative intensity I vs. range r; same as in Fig. 6 except $f = 20$ Hz.

FIG. 8. Relative intensity I vs. range r; same as in Fig. 6 except $f = 40$ Hz.

FIG. 9. Relative intensity I vs. range r; same as in Fig. 6 except $f = 80$ Hz.

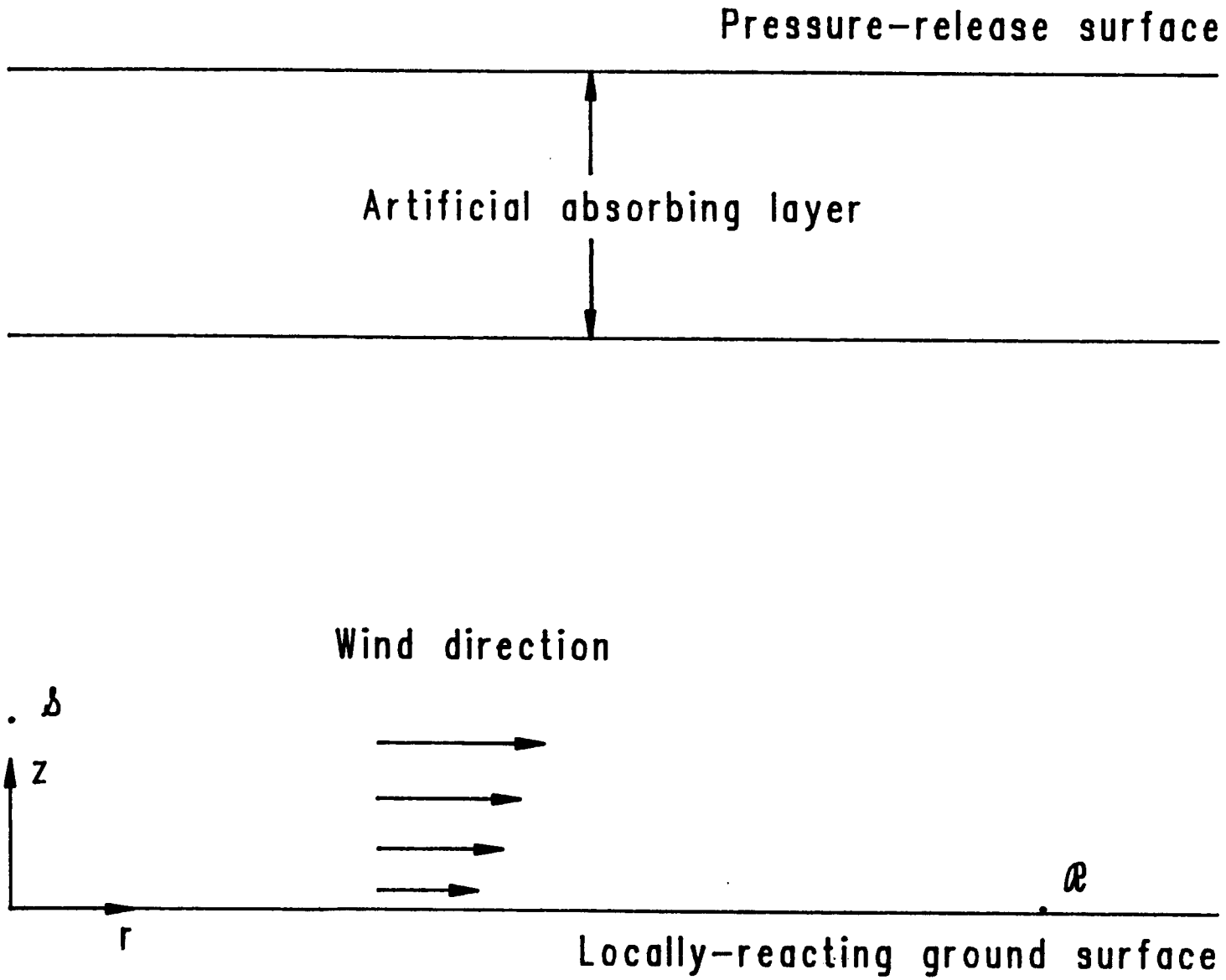

Robertson et. al. FIG. 1

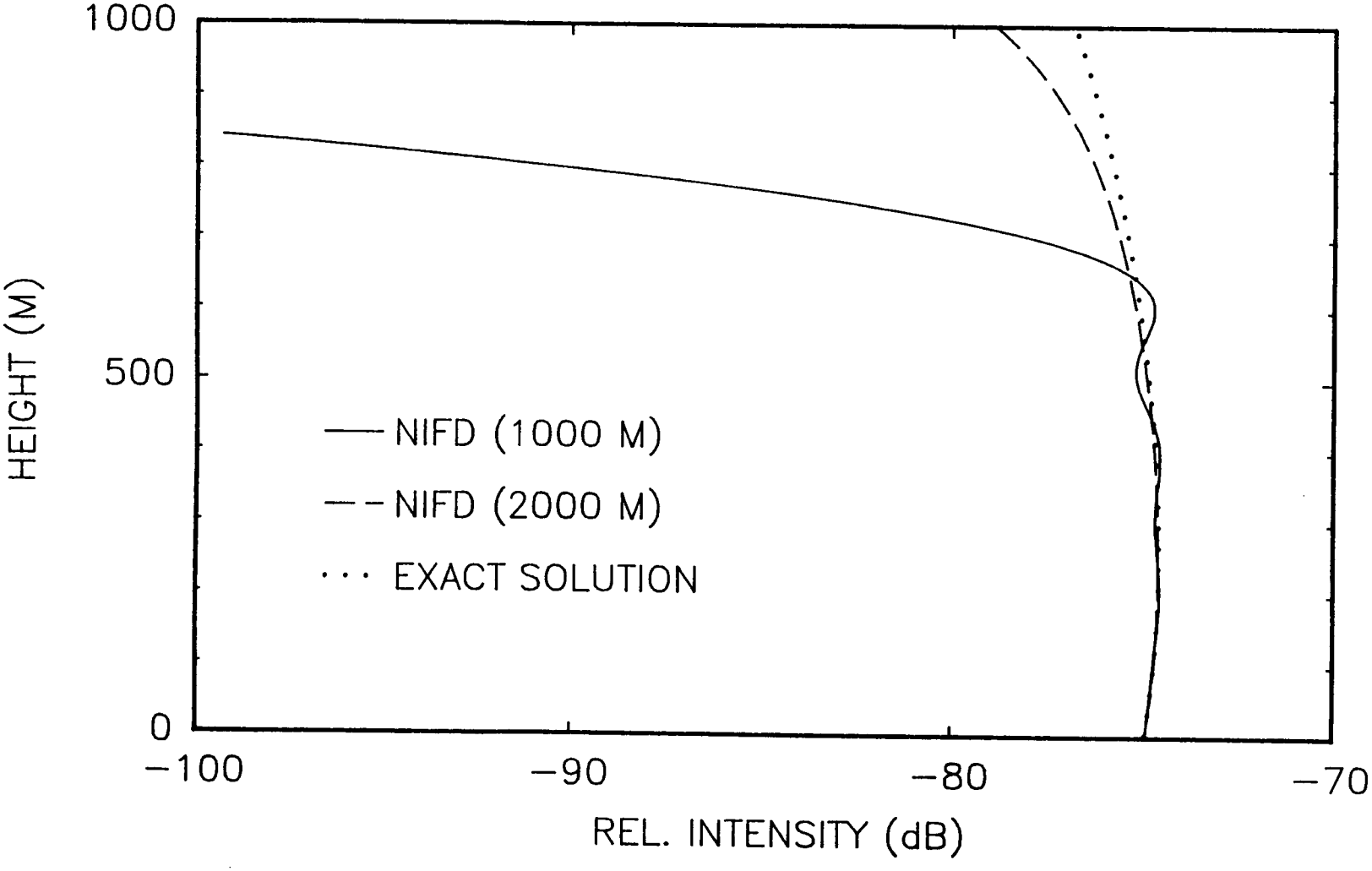

Robertson et. al. FIG. 2

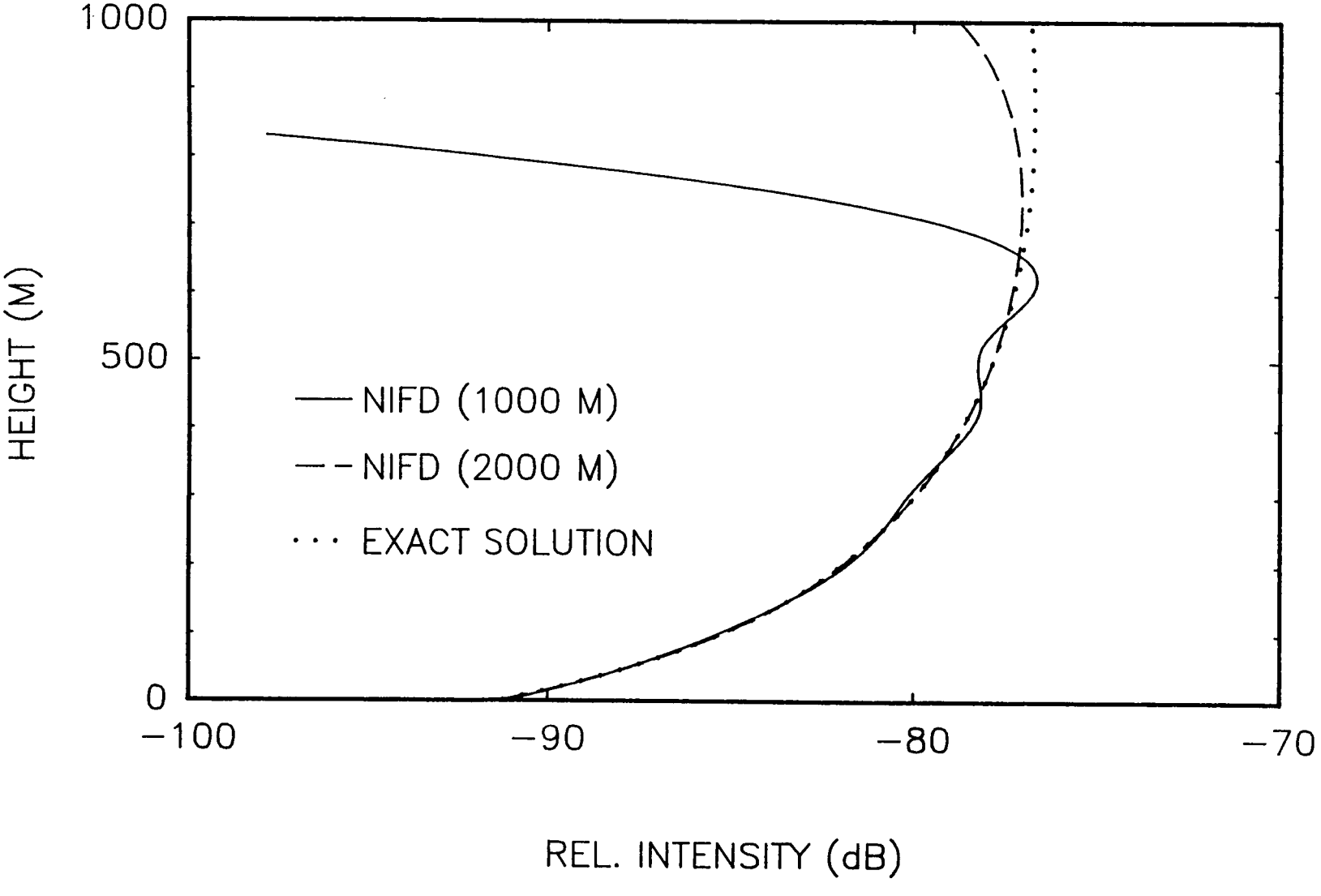

Robertson et al. FIG. 3

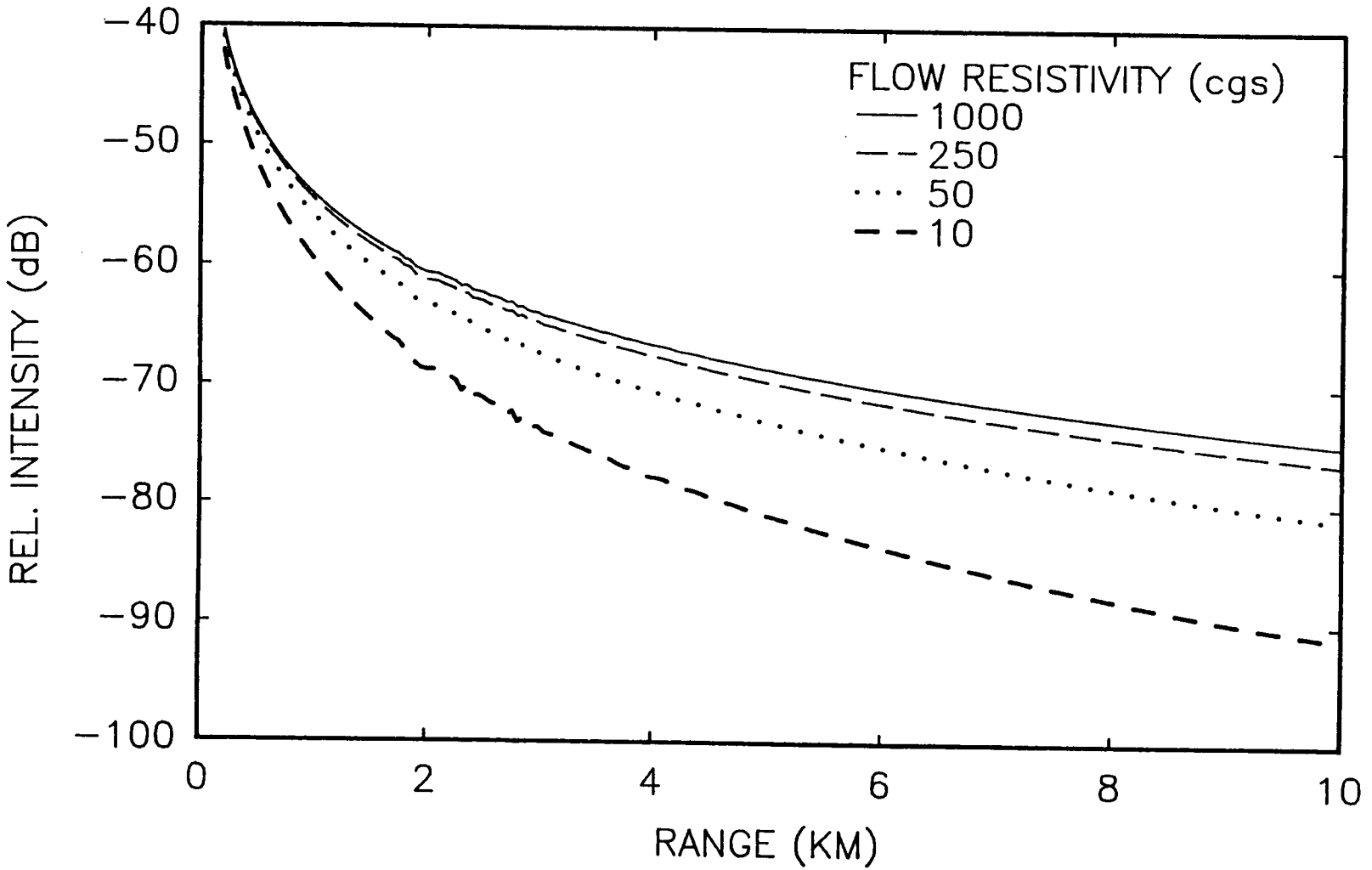

Robertson et al. FIG. 4

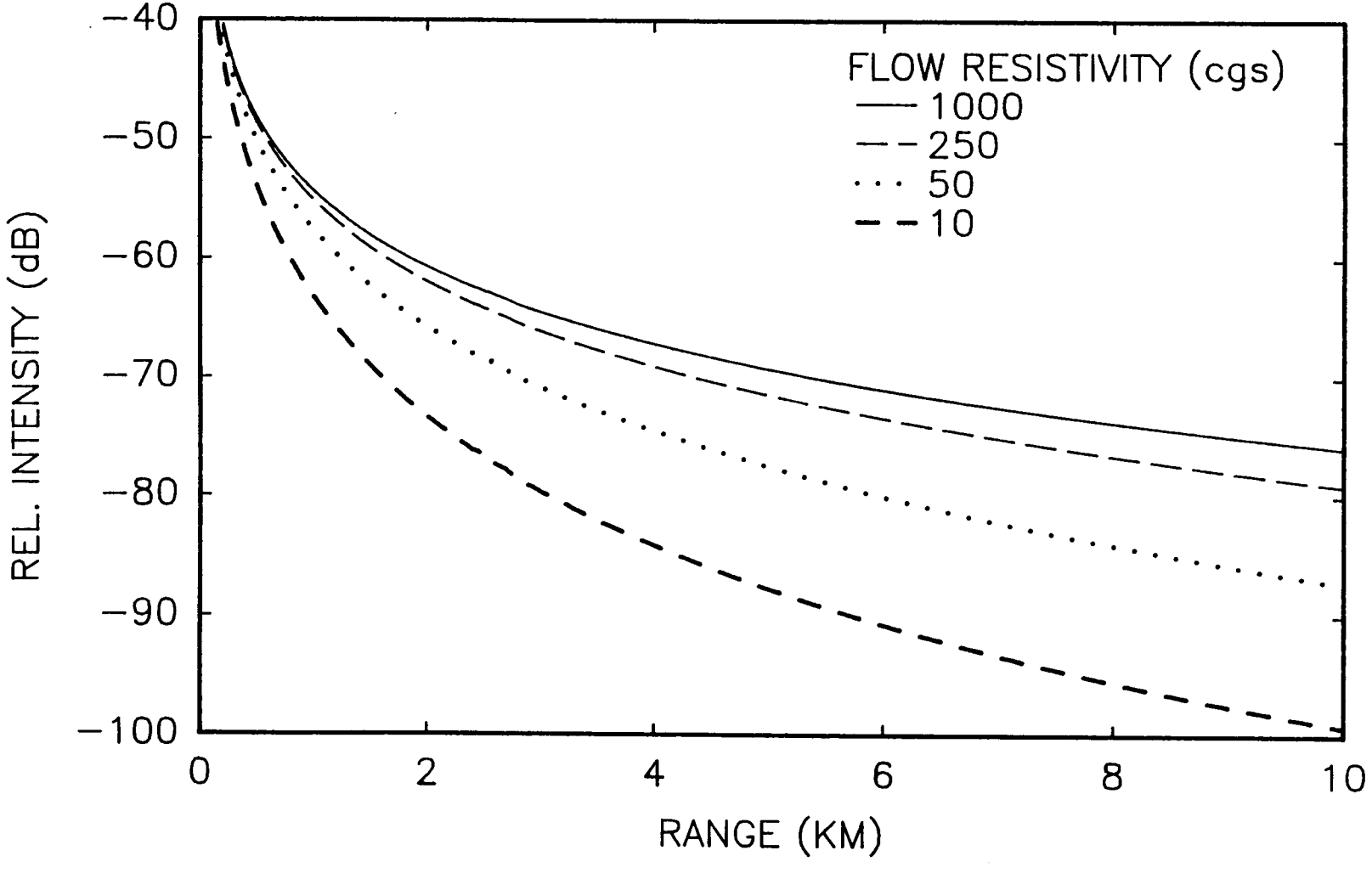

Robertson et al. FIG. 5

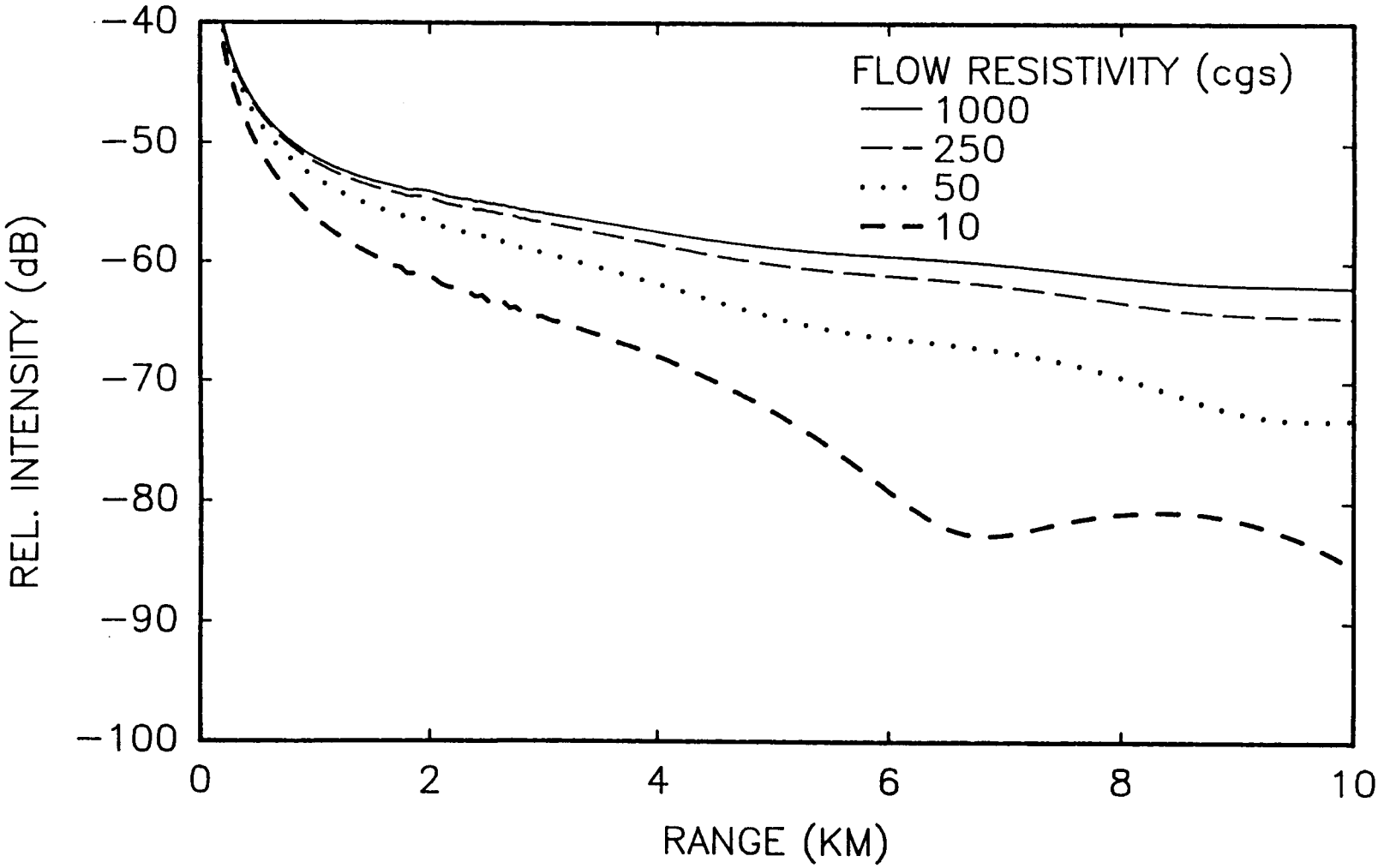

Robertson et al. FIG. 6

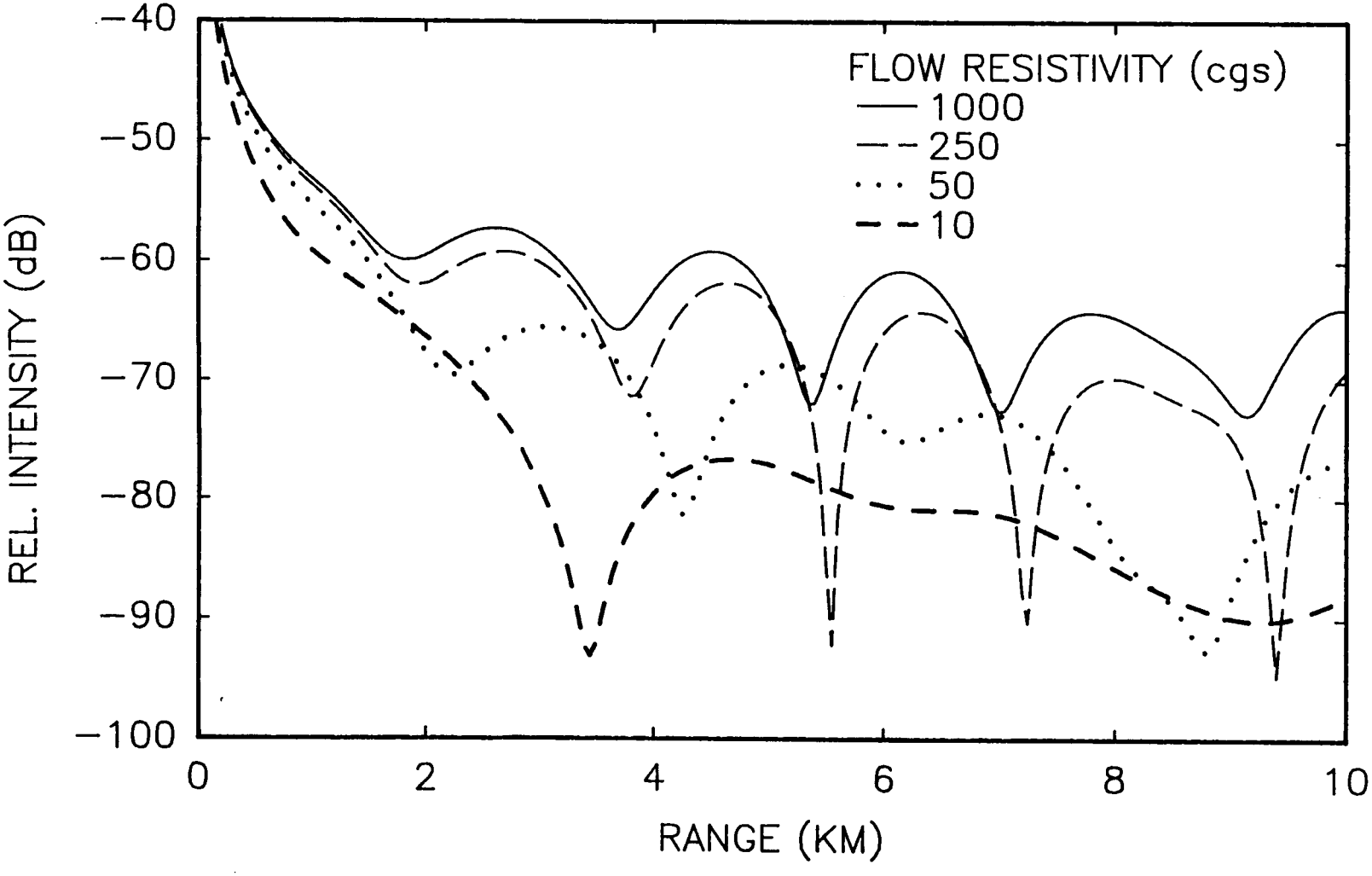

Robertson et al. FIG. 7

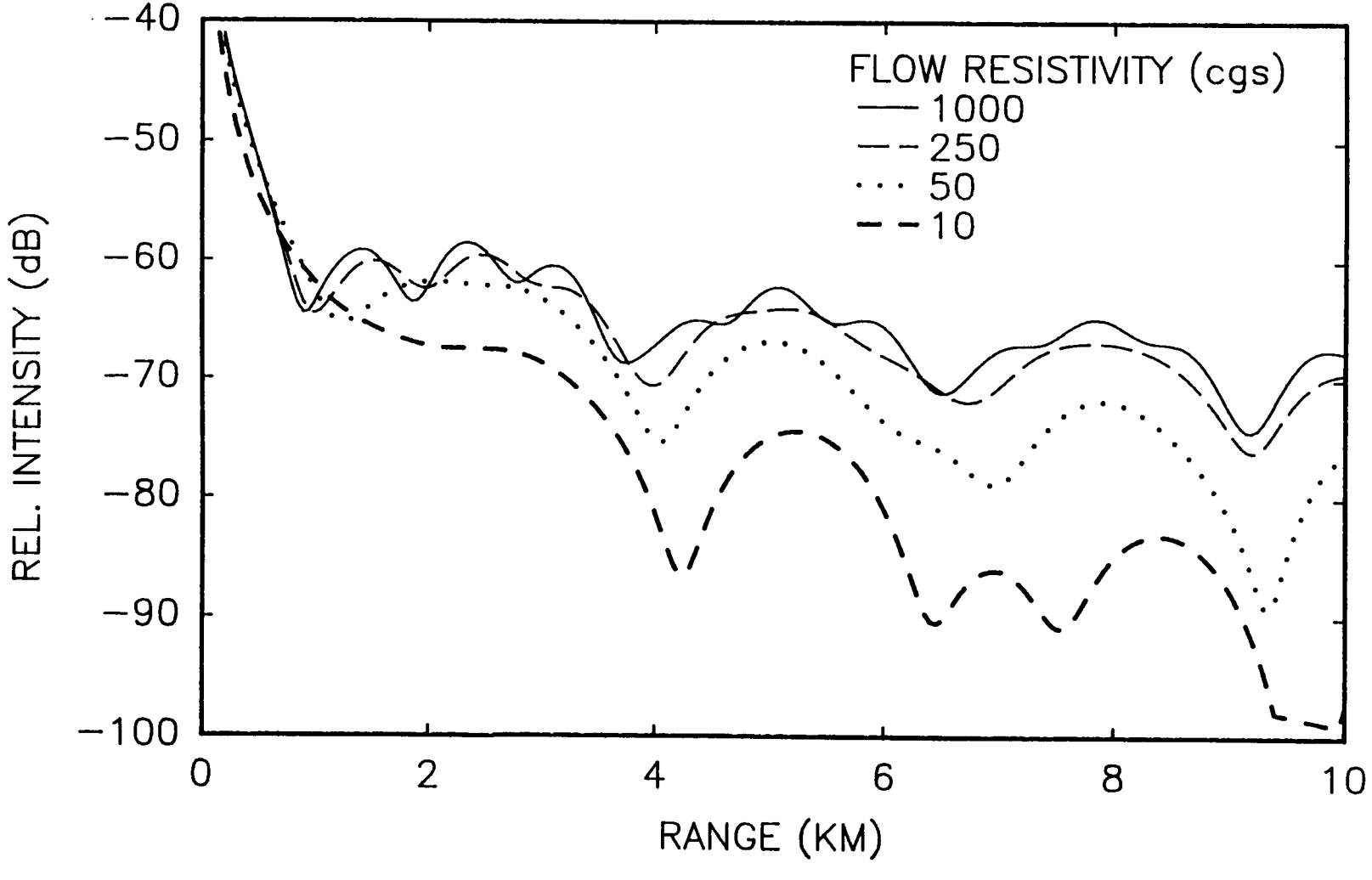

Robertson et al. FIG. 8

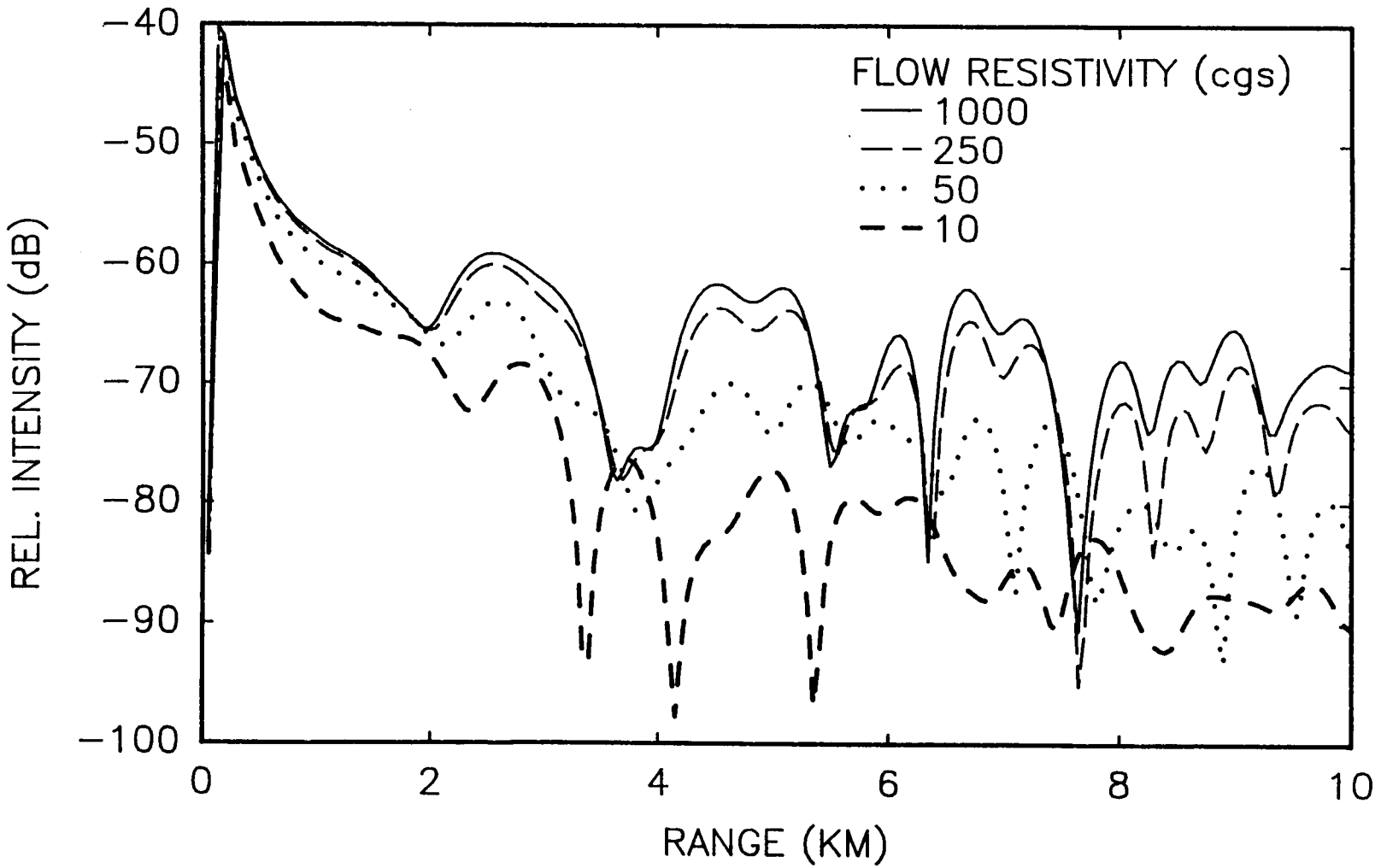

Robertson et al. FIG. 9

Distribution List:

NASA Langley Research Center, Applied Acoustics Branch, MS 460, Hampton, VA 23665
ATTN: Dr. Gary McAninch 3
ATTN: Mr. Arnold Mueller 1
ATTN: Mr. David Chestnutt 1

NASA Scientific and Technical Information Facility, P.O. Box 8757, Baltimore-Washington International Airport, MD 21210 2

U.S. Army Laboratory Command, ATTN: SLCTO (Dr. Norman Berg), 2800 Powder Mill Road, Adelphi, MD, 20783-1145 1

U.S. Army Atmospheric Sciences Laboratory, ATTN: SLCAS-AR-A (Dr. Richard Shirkey), White Sands Missile Range, NM 88002-5501 1

U.S. Army Research Office, Mathematical Sciences Division (Dr. Jagdish Chandra), P.O. Box 12211, Research Triangle Park, NC 27709 1

Office of Naval Research, Code 1125OA (Dr. Marshall Orr), 800 North Quincy Street, Arlington, VA 22217-5000 1

Naval Underwater Systems Center, Code 3122 (Dr. Ding Lee), New London, CT 06320 1